We are IntechOpen, the world's leading publisher of Open Access books Built by scientists, for scientists

6,900
Open access books available

185,000
International authors and editors

200M
Downloads

Our authors are among the

154
Countries delivered to

TOP 1%
most cited scientists

12.2%
Contributors from top 500 universities

WEB OF SCIENCE™

Selection of our books indexed in the Book Citation Index in Web of Science™ Core Collection (BKCI)

Interested in publishing with us?
Contact book.department@intechopen.com

Numbers displayed above are based on latest data collected.
For more information visit www.intechopen.com

13

Simulation of Subject Specific Bone Remodeling and Virtual Reality Visualization

Ajay Sonar, Laurel Kuxhaus and James Carroll
Clarkson University
U.S.A.

1. Introduction

Bone is a dynamic tissue. The dynamic nature is the result of the remodeling process, in which the skeleton is renewed continuously. The external mechanical loading affects the remodeling process which in turn affects the internal structure. German anatomist Julius Wolff first noticed this phenomenon in 1892 (Wolff, 1986). The purpose of remodeling is to prevent the accumulation of damage, adapt the internal architecture to the external loads and maintain homeostasis (Van Der Linden et al., 2001; Pivonka et al., 2008; Lemaire et al., 2004).
Compressive fractures caused by osteoporosis are common in the lower vertebrae is a frequent region for compressive fracture due to osteoporosis (Melton et al.,1989; Melton et al.,1999; Scane,1994). Figure 1 shows the overall structure of a lumbar vertebrae. The outer dense bone is called cortical bone and the inner porous bone is called cancellous bone. To understand the remodeling process it is important to understand the role of the cells involved in the process. Osteoblasts are the cells responsible for the bone formation. They have a single eccentric nucleus. Osteoclasts are multi-nucleated cells responsible for bone resorption. Together they are called the Basic Multicellular Unit (BMU). During bone formation some of the osteoblasts get trapped in the matrix that they secrete and become Osteocytes. Another type of cells are lining cells which cover the entire bone surface. These are quiescent osteoblasts. The osteocytes are connected to each other (Figure 2) and to the lining cells through narrow channels called the Canaliculi (Parfitt, 1984).
Remodeling involves the coordinated actions of osteoclasts, osteoblasts, osteocytes and bone lining cells. The remodeling process involves removal of packets of bone from the surface followed by formation of new bone within the cavity created. This is a cyclic process involving five stages - quiescence, activation, resorption, reversal, formation and back to quiescence. Remodeling happens in adult animals. In younger animals in which the bone is still growing the process is called modeling. The fundamental difference between the two processes is that the remodeling is a cyclic process of erosion and formation on the bone surface, whereas in modeling, either bone resorption or formation occur continuously for a long period of time without interruption (Parfitt, 1984). In adults, bone is continuously remodeled at discrete locations. The balance between bone resorption and formation determines the bone mineral content.
Osteoclast activity determines the extent of the depth of resorption and the osteoblast activity controls the amount of bone formation. The osteocytes, with their interconnected cellular network, play an important role in communication and transportation between cells within the bone matrix. When there is a balance between the bone formation and bone resorption

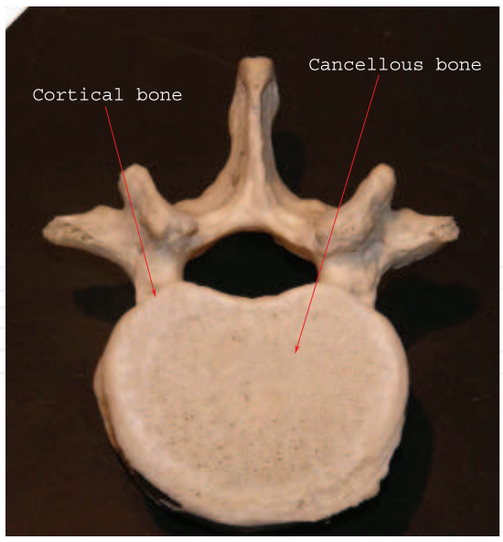

Fig. 1. Transverse view of a lumbar vertebrae (http://biology.clc.uc.edu/Fankhauser/)

there is no bone loss. In younger animals the rate of bone formation is more than bone resorption, hence the bone mass keeps increasing. In adults this process reaches a steady state therefore there is no significant change in the bone mass but the geometry keeps changing. In older animals the rate of bone resorption is more than bone formation which results in bone loss. The process of remodeling is illustrated in Figure 3 (Parfitt, 1984).

The osetocytes and the canalicular network play an important role in the modeling and remodeling process. Osteocytes act as load sensors. Frost proposed that a minimum effective strain (MES) is required to trigger remodeling (Frost, 1983). According to the supporting experiments the range of MES was determined to be 0.0008-0.002 unit bone surface strain. Strains below MES do not evoke modeling and strains above do. Since the maximum deformations in bone tissue are relatively small, another theory suggest that bone cells respond to stress generated flow of interstitial fluid through the canalicular network, which transmit this information to other osteocytes and to the lining cells (Weinbaum et

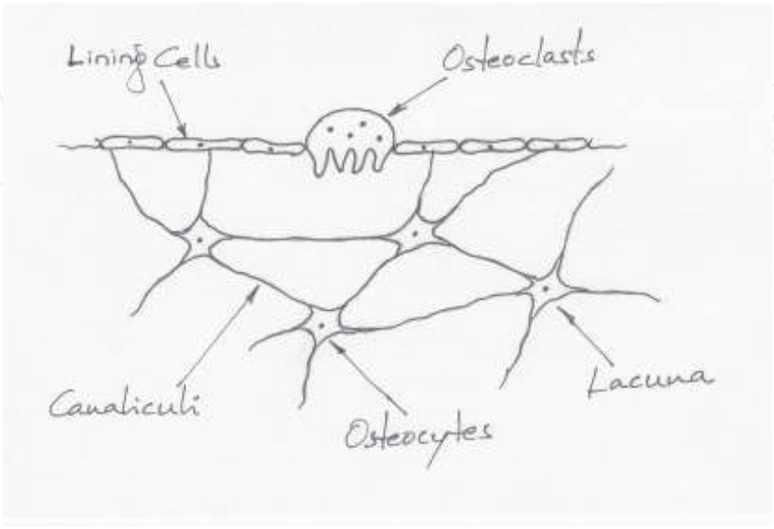

Fig. 2. Bone cells

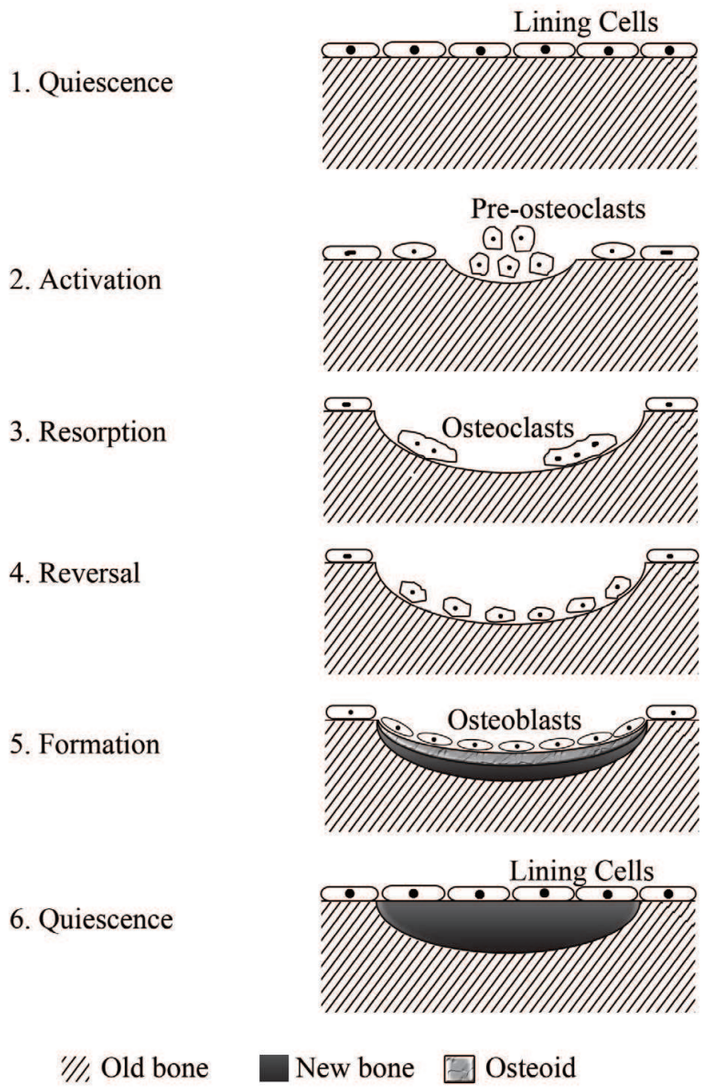

Fig. 3. Remodeling cycle in adult bone (Parfitt, 1984)

al.,1994; Turner et al.,1995). The response to overuse or disuse is formation or resorption respectively. When the osteocytes sense a mechanical stimulation which is more than the normal physiological use, they send signals to the lining cells and more osteoblasts cells are recruited. These osteoblast form new bone on the surface in that area which restores the normal level of use. Disuse reduces the stress and also transportation of nutrients. This will cause the death of osteocyte, which is a signal to recruit new osteoclasts (Bronckers et al., 1996). This process is illustrated in Figure 4(a) (Burger & Klein-Nulend, 1999).

Remodeling also occurs due to fatigue damage. Fatigue damage occur due to repetitive loading in the normal physiological range. When accumulated over time they result in microcracks. These micro cracks run through the mineralized matrix, which may disrupt the canalicular network and the osteocytes. This creates a situation similar to disuse in which the communication between the osteocytes and the bone lining cells is severed, resulting

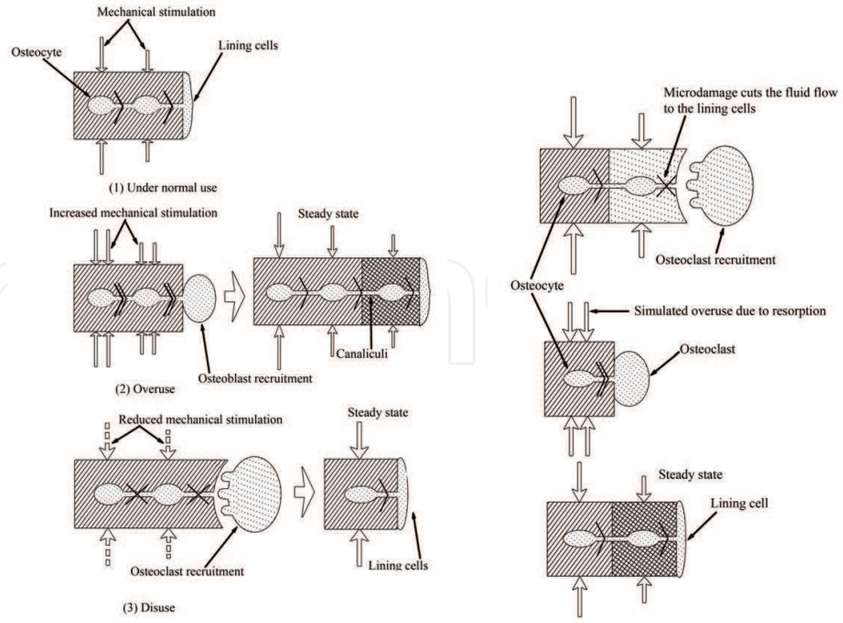

Fig. 4. (a)Schematic representation of bone modeling and (b) Schematic representation of bone remodeling due to microdamage (Burger & Klein-Nulend, 1999)

in osteocyte recruitment. Osteoclast resorb the damaged bone until the undamaged bone is reached. The local loss of bone results in local overuse of the remaining bone. The resulting increased fluid flow through the canalicular network triggers the recruitment of osteoblasts. The osteoblasts build the bone matrix until a steady state is reached. This is illustrated in Figure 4(b).

The trajectorial hypothesis put forward by Wolff (Wolff, 1986) suggests that the architecture of the bone is transformed to align the trabeculae with the principal stress orientation. Remodeling, also called as maintenance, is an adaptive process which is regulated by the bone cells influenced by the local state of stress. The proposed hypothesis in this study is as follows: by appropriately simulating the external loading conditions on the bone a more realistic change in the geometry of trabecular structure can be estimated.

2. Literature review and present work

The bone is continuously being remodeled. This occurs at multiple spatially and temporally discrete sites. It happens in both the trabecular bone and the cortical bone. This prevents the accumulation of damage (Burr, 1993), helps in adapting the architecture to external load and provides a way for the body to alter the balance of the essential minerals by accessing the stores of calcium and phosphate (Burr, 2002). Bone goes through a continuous process of modeling in younger animals. It reaches a peak mass at approximately 30 years of age and decreases gradually after that (Van Der Linden et al., 2001). This decrease in mass is caused by the formation deficit, the osteoblast formation is less relative to osteoclast resorption. The remodeling process as described by Parfitt (Parfitt, 1984) is illustrated in Figure 3. Normally 80% of the bone surface is quiescent with respect to remodeling. Activation requires recruitment of osteoclasts, a means for them to gain access to the bone and a mechanism

to attach to the bone surface. Activation is a function of age, sex and metabolic state. It occurs partly at random and partly in response to the biomechanical requirement. After coming in contact with the bone, the osteoclasts begin to resorb the bone. It is referred to as Howship's lacuna in trabecular bone and as cutting cone in cortial bone. The resorption cavity has a charecteristic shape and dimension. The resorption cavity grows at a rate of 5-10μm/day perpendicular to the surface and 20-40μm/day parallel to the surface. After the resorption ends, it enters a reversal phase. The rough surface of the resorption cavity is smoothed and thin layer of highly mineralized matrix is laid down, preparing the surface for bone formation. Once the surface is ready, osteoblast cells are recruited. This phase has two parts, matrix synthesis and mineralization. Mineralization follows matrix synthesis. The newly laid unmineralized bone matrix is called osteoid. This seperates the osteoblasts and the newly mineralized bone. Synthesis terminates after the cavity is filled. Mineralization continues slowly until the osteoid seam disappears. The osteoblasts that remain on the surface transform in to lining cells.

Bone adapts its structure much more readily during growth than after skeletal maturation because it is intrinsically responsive to strain (Frost, 1982). During modeling there is no need for activation of the surface since it is continuously active from earliest embryonic stage until growth ceases. Whereas in the adult bone, for the adaptive change to occur, the quiescent surface needs activation.

Unlike cortical bone which is dense, trabecular bone is porous and extremely anisotropic. It consists of numerous interconnected struts mostly with thick vertical struts and thinner horizontal struts. There are two distinct types of struts present in the structure, plates and rods. As the name suggest the rods are more cylindrical and long whereas the plates are more flat. In a study on the age related change by Mosekilde (Mosekilde, 1988; 1989), on individuals between the age of 15 to 87, a significant thinning and disappearance of the horizontal supporting struts and total removal of some of the vertical struts were observed. A significant increase in both the horizontal and vertical trabecular distance was also shown. A pronounced loss of bone strength was shown in females around the age of 40-50 (Mosekilde, 1989).

Many theoretical and computational models have been proposed to investigate and simulate the dynamic behavior of the bone (Van Der Linden et al.,2001; Lemaire et al.,2004; Thomsen et al.,1994; Langton et al.,1998). With high resolution imaging methodologies such as μCT becoming more accessible, the study of trabecular remodeling began to take in to account the influence of cellular activity in 2 and 3 dimensions (Liu et al., 2008; Van Der Linden et al., 2001; Müller & Hayes, 1997). Simulation involving effect of metabolic bone formation deficit and the micro structural bone formation deficit are also developed (Van Der Linden et al., 2001; Linden et al., 2003). Effect of trabecular plate thickness and the trabecular plate density on the age related changes showed that the plate density is more significant predictor of bone loss than a decrease in the plate thickness (Parfitt et al., 1983).

Different mathematical control models of mechanical bone mass regulation have been proposed (Cowin & Hegedus,1976; Mullender & Huiskes,1995; Huiskes et al.,1987). These models assumed a continuous feedback loop between the maintenance of bone mass and local strain values in the tissue. This enabled mathematical predictions of local bone regulation based on external loads. These models differ in the kind of mechanical signal used to control the feedback loop. Finite element methods are used to link the external loads to local mechanical signal. These models were validated to produce accurate prediction of long term formation and resorption (Van Rietbergen et al., 1993; Weinbaum et al., 1994). The results of

these models showed that the orientation of the trabeculae is directly related to the external principal stress orientation, and when the orientation of the principal stress is rotated the trabecular architecture transformed to realign to the new orientation.

Apart from the visual assessment of the structural changes, different structural parameters are used to characterize these changes (Parfitt et al., 1987; Müller & Rüegsegger, 1996; Müller & Hayes, 1997; Liu et al., 2008). In the past, these parameters were studied by the examination of the two dimensional crossections of cancellous bone biopsies. The three dimensional morphometric parameters are then derived from two dimensional images using stereological methods (Parfitt et al., 1987). The bone volume fraction,which is a ratio of bone volume to the total volume of the structure (BV/TV), and the surface density, which is the ratio of the bone surface area to the bone volume (BS/BV), can be obtained directly from the two dimensional images, whereas trabecular thickness (Tb.Th), trabecular separation (Tb.Sp) and the trabecular number (Tb.N) are derived indirectly assuming a fixed structural model. Typically an ideal plate or rod model is assumed. The problem with this method is that, it will lead to errors in the indirectly derived parameters if the structure deviates from the assumed model. It has been shown that the error due to deviation could be up to 52% depending on the method used (Simmons & Hipp, 1997). Cancellous bone structure continuously changes is structural type. Since the stereological method assumes a certain structural model, the initial parameters calculated on a trabecular bone undergoing remodeling cannot be compared with the subsequent calculated parameters because the remodeling changes the type of the structure from plate-like to rod-like (Hildebrand & Ruegsegger, 1997). Recent advances in μCT have made it possible to acquire these parameters directly from 3D μCT image (Hildebrand et al., 1999) without any underlying model assumptions. The values obtained by this method were shown to correspond well with the stereological method (Thomsen et al., 2005). The trabecular thickness is determined by filling maximal spheres into the structure, then the average thickness of all points in the bone is calculated to give Tb.Th (Hildebrand & Ruegsegger, 1997). The Tb.Sp is calculated in the same way but the points representing the non bone region or the marrow region are used to fill the maximal spheres (Hildebrand et al., 1999). The Tb.N is taken as the inverse of the mean distance between the midaxis of the trabecular structure. The calculated midaxes of the cancellous structure can also be used to decompose the bone in to rods and plates (Stauber & Müller, 2006; Ju et al., 2007). Further, the orientation of the rods can also be calculated. By decomposing the cancellous bone in to rods and plates, the trabecular thickness can be calculated for the rods and plates seperately. A comparison between the indirect calculated values assuming fixed model structure and the model independent direct calculation is made in (Hildebrand et al., 1999).

The idea proposed in this research is the use of the realistic mechanical loading data to run a remodelling algorithm to predict the structure of trabecular bone after real-world loading conditions are applied. This can be achieved by gathering the motion capture data of an individual performing different activities (eg., walking, running, lifting weights etc.). These activities can be grouped into different categories like easy, medium or hard based on their intensity. This data can be collected with any motion capture system. This data can be used in virtual human modeling and musculoskeletal simulation software to calculate forces and displacements at various joint locations or at specified marker locations. This force data is then used in the remodeling algorithm to accurately predict the modified trabecular structure. This data could be useful to predict and change the lifestyle/physical habits to avoid severe chronic damage/injury. The schematic of the proposed method is shown in the Figure 5.

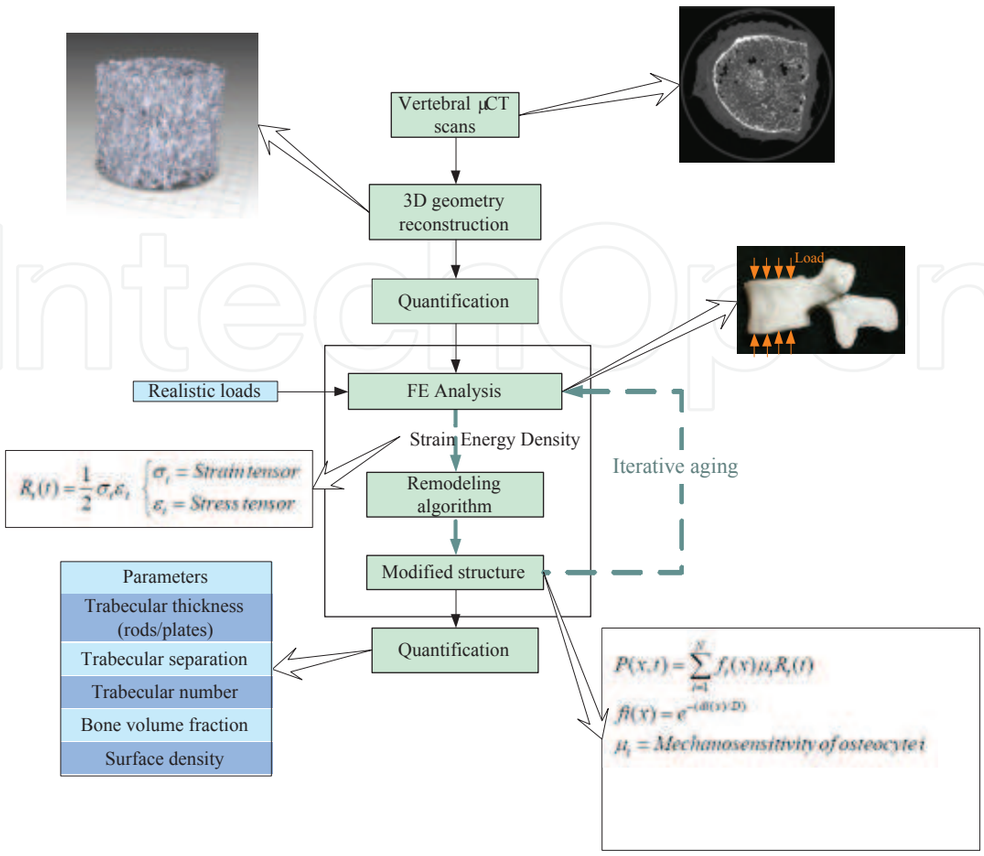

Fig. 5. Schematic of the proposed method

3. Materials and methods

For this study μCT images of fourth lumbar vertebrae (L4) were used. The original μCT images have a resolution of 18μ x 18μ x 36μm. The steps involved in the simulation process are outlined below.

3.1 Image processing

This step involves reading the images, thresholding, segmentation and 3D geometry reconstruction. In the initial phase of the project, a core of the vertebra was used instead of the entire vertebra. The region of interest (ROI) was chosen to be at the center of the vertebra to avoid artifacts present at the edges during scanning. Because of the physical limitation on the size of the specimen that can be physically manufactured and tested for another part of the project, the ROI was chosen to be 480 pixels in diameter. The aspect ratio (diameter/height) of a single vertebral body is 1.33. To maintain this aspect ratio in the cored sample, a total of 384 images were chosen from the entire set. These cored images were then thresholded to separate the bone matrix form the surrounding marrow. Each image is thresholded individually with a value of 22.4% of its maximal gray value (Rüegsegger et al., 1996).

Once all the images are segmented and thresholded, the next step is to construct the 3D geometry from them. 3D geometry can be represented in many ways. One way is to store a list of vertices on the surface and a list of indices that form connected triangular facets from

those vertices. An isosurface algorithm is used to extract this information. The images are stored in a three dimensional array. The isosurface algorithm connects the points that have a value equal to the one specified by the user, which is called the isovalue. In this experiment, the pixels in each image have two values, 0 for marrow or the pixels in the background space and 1 for the region that represents the bone. Hence an isovalue of 1 would generate a list of points on the surface of the bone along with a list of combination of indices that form triangular facets.

3.2 Quantification

The parameters selected to quantify the bone structure are, bone volume fraction which is a ratio of bone volume to the total volume (BV/TV), surface density which is the ratio of bone surface area to the bone volume (BS/BV), trabecular thickness (Tb.Th), trabecular separation (Tb.Sp) and the trabecular number (Tb.N) (Hildebrand et al., 1999). The bone volume (BV) is the volume enclosed by the bone surface. Total volume (TV) is the volume of the bone including the marrow space. The bone surface area is calculated by adding the area of all the triangles, generated by the isosurface function, forming the surface. The area of a triangle formed by its vertices a, b, and c is give by equation 1.

$$\begin{aligned} A &= a - b \\ B &= c - a \\ Area &= (A \times B)/2 \end{aligned} \tag{1}$$

Since the bone geometry is irregular it is difficult to calculate the volume of it and there are different ways this can be accomplished. One way to overcome this problem is to chop the whole geometry in to smaller known geometry and add the volume of each element. The 3D geometry representing the bone volume is split in to tetrahedral mesh elements using a tetrahedral mesh generation algorithm (*http://iso2mesh.sourceforge.net/cgi-bin/index.cgi*, Nov 2010). The volume of the bone is the sum of the volume of all the tetrahedral elements (Sommerville, 1959). Another reason to split the geometry in to tetrahedral elements is that this information can be used in the later stage of the project in the stress analysis using finite elements techniques. The volume of an irregular tetrahedron is calculated using the following equation 2

$$\begin{aligned} D &= \begin{bmatrix} 0 & u^2 & v^2 & w^2 & 1 \\ u^2 & 0 & W^2 & V^2 & 1 \\ v^2 & W^2 & 0 & U^2 & 1 \\ w^2 & V^2 & U^2 & 0 & 1 \\ 1 & 1 & 1 & 1 & 0 \end{bmatrix} \\ Volume &= \sqrt{\det(D)/288} \end{aligned} \tag{2}$$

where (U,u), (V,v) and (W,w) are opposite edge length pair, illustrated in the Figure 6.
Before calculating the other three parameters, an additional step of calculating the medial axis of the structure is introduced. A medial axis is a plane for a plate like structure and a line for a rod like structure (Figure 7). A voxel model of the bone structure is constructed. A voxel is a three dimensional pixel element, i.e. a cube of user specified dimensions. The voxel reconstruction is performed by first building a voxel space that is approximately the same

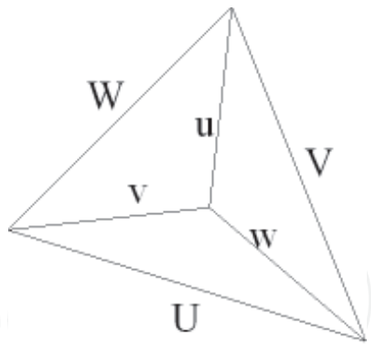

Fig. 6. Edge lengths for calculation of volume

size as the specimen. The size of the voxel element defines the resolution of the final model, i.e., smaller the voxel, higher the resolution. Each layer of the voxel form the voxel space is projected on to the binary μCT scan. The voxels that intersect the cancellous bone region, i.e., the white region in the binary images, are retained and the rest are discarded. After this process is repeated on all the images, the remaining voxels represent the volume of the specimen. The calculation of the medial axis is an iterative algorithm where in each iteration the boundary voxels of the structure is calculated. Each of these voxels are tested to see if it is a critical point. If the removal of a particular boundary voxel changes the topology of the structure then it is tagged as critical. The other non-critical voxels are removed. This process is repeated until there are no more voxels to be removed. The result of this algorithm is a set of voxels representing the skeleton of the structure. This can be further broken down in to set of points representing the skeleton of the rods, called curves, and a set of points representing the skeleton of the plates, called surfaces. The advantage of this addition step is that, the medial axis can be used to separate each individual trabecule and to calculate the orientation of these trabeculae. This information is useful in the simulation because studies have shown that the orientation of the trabeculae affects the age related thinning process (Mosekilde, 1988; 1989).
The direct 3D method is used to calculate the trabecular thickness (Tb.Th). Maximal spheres are fitted to every point in the structure and take the mean to calculate the mean thickness. For efficient implementation of the algorithm distance map for every point in the structure is calculated by the distance transformation, which assigns euclidean distance from that point to the nearest background point. The mean of these values give the mean trabecular distance. The trabecular thickness of the rods and plates can be calculated separately to study the effects

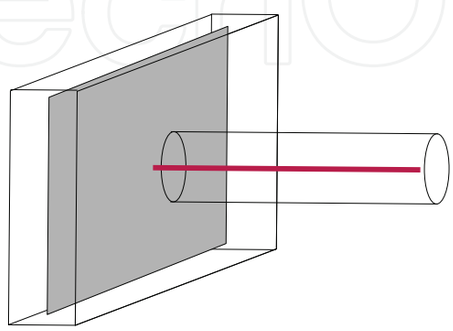

Fig. 7. Medial axis: Shaded gray area represent the mid plane of the plate and the red line represents the mid axis of the rod like structure

of the age related thinning on them. The trabecular separation is calculated in the same way, but on the background voxels. The background voxels are calculated by finding the background pixels on each slice of the image. For this, the convex hull of each image slice is calculated. The pixels representing the bone area are removed from this convex hull. The remaining pixels represent the background pixels. Once this process is repeated on all the image slices the voxel model representing the background is constructed. The same process of calculating the trabecular thickness is repeated on these background voxels which give the trabecular separation (Tb.Sp). A slight modification of the process of the trabecular separation give trabecular number. Maximal spheres are fitted to the background voxels, but this time the boundary of the sphere is not to the surface of the bone, but all the way till the mid-axis of the trabecular structure. The inverse of this value give trabecular number and is defined as the number of plates per unit length (Hildebrand et al., 1999).

3.3 Simulation using finite element methods

Osteocytes located within the bone matrix measure the mechanical signal, the strain energy density rate, which is the result of recent loading history. They stimulate the actor cells (osteoblasts and osteocytes) within their vicinity to adapt the bone mass depending on the difference between the measured signal and the reference signal. The influence of the ostecytes on its environment is decreases exponentially with increase in distance from the actor cells. This relation is given by the following equation (Mullender & Huiskes, 1995)

$$f_i(x) = e^{-(d_i(x)/D)} \tag{3}$$

where d_i(x) is the distance between osteocyte i and location x. The parameter D is the distance from osteocyte i to the location where its effect has reduced to e^{-1} or 36.8%.

The relative density of the bone at location x is controlled by the stimulus value P(x,t), to which all the osteocytes within the vicinity contribute, based on the distance relationship. This is given by the following equation (Mullender & Huiskes, 1995; Huiskes et al., 2000)

$$P(x,t) = \sum_{i=1}^{N} f_i(x)\mu_i R_i(t) \tag{4}$$

where μ_i is the mechanosensitivity of the osteocyte i, and $R_i(t)$ is the strain energy density rate at osteocyte location i. The local change in the relative density of the bone m is expressed as (Huiskes et al., 2000),

$$\frac{dm}{dt} = \begin{cases} \tau\{P(x,t) - k_{th}\} - r_{oc} & \text{for } P(x,t) > k_{th} \\ -r_{oc} & \text{for } P(x,t) \leq k_{th} \end{cases} \tag{5}$$

where k_{th} is the threshold of bone formation, r_{oc} is the relative amount of bone resorbed by osteoblasts and τ is the time constant regulating the rate of the process. The relative density of the bone varies between 0 (for no bone) and 1 (for fully mineralized bone). It is assumed that the osteocytes disappear at location where the mineral density goes to 0 and new osteocytes are formed at locations where the density reaches 1. The resorption is regulated by the presence of micro cracks or by disuse (Huiskes et al., 2000; Ruimerman et al., 2001). In this work, resorption due to the presence of micro cracks is assumed to be constant.

$$p(x,t) = d \quad (spatially\ random) \tag{6}$$

Resorption due to disuse is dependent on the strain and is given by the following equation,

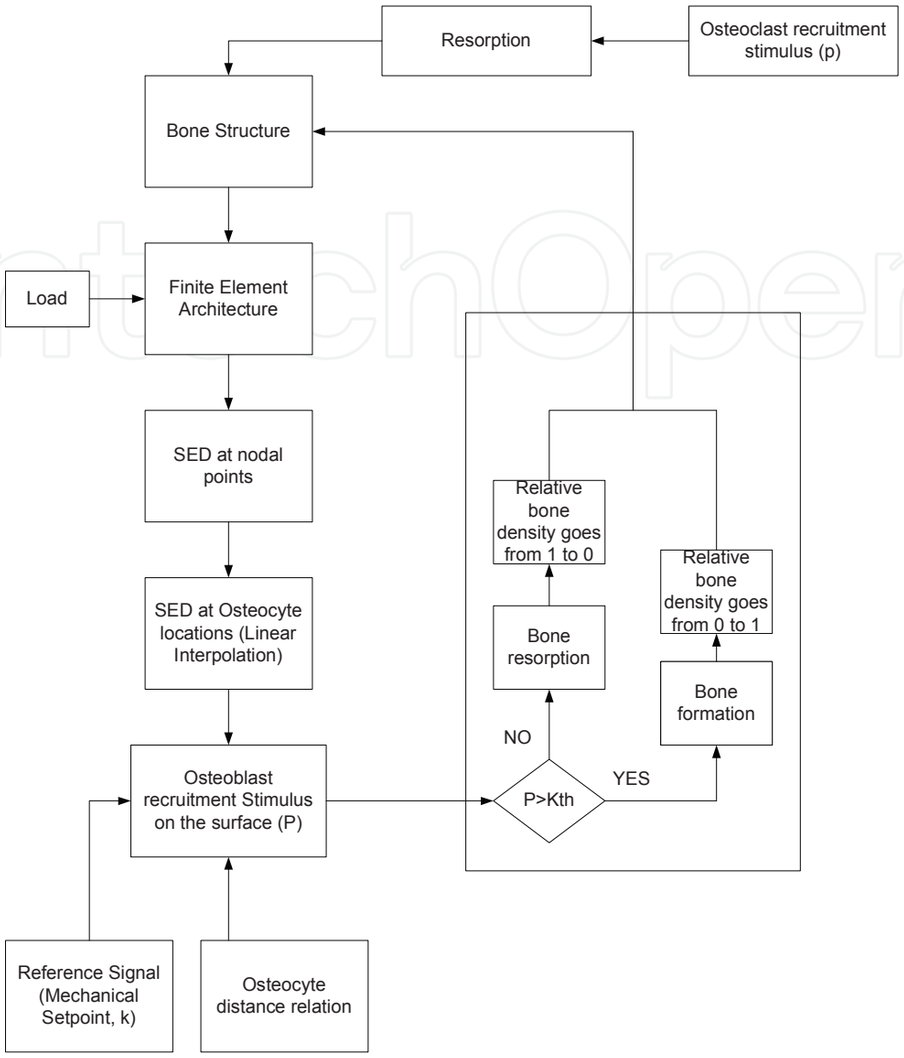

Fig. 8. Regulatory mechanism for Wolff's Law

$$p(x,t) = \begin{cases} c[a - P(x,t)] & \text{if } P < a, \\ 0 & \text{if } P \geq a \end{cases} \tag{7}$$

where $c = 12.5$ and $a = 1.6$.

This entire process of regulation of the bone mass and architecture is illustrated in the block diagram in Figure 8.

The objective is to supply the load information to the algorithm which is representative of realistic everyday activity by a person. Due to the size of the data and the time consumed to process it, it is intended to use the parallel computing functionality of the Matlab software on a cluster of machines.

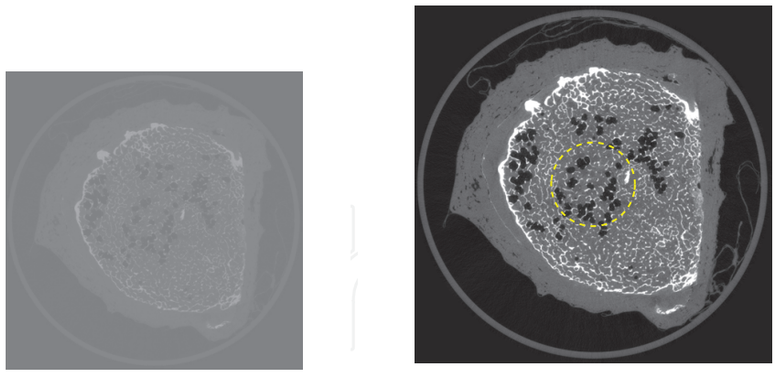

(a) (b)

Fig. 9. (a)Original μCT scan (b)Enhanced CT scan showing the ROI

4. Results

4.1 Image processing

The original μCT scan is shown if Figure 9(a). The region of interest (ROI) is shown in Figure 9(b) by the yellow circle.

Figure 10(a) shows the cored images and Figure 10(b) shows the thresholded core image. The thresholded core images are stored in a 3D image matrix. An isosurface algorithm is used to generate the surface geometry of the bone with an isovalue of 1. The result of this is a 3D surface geometry which is shown in Figure 11.

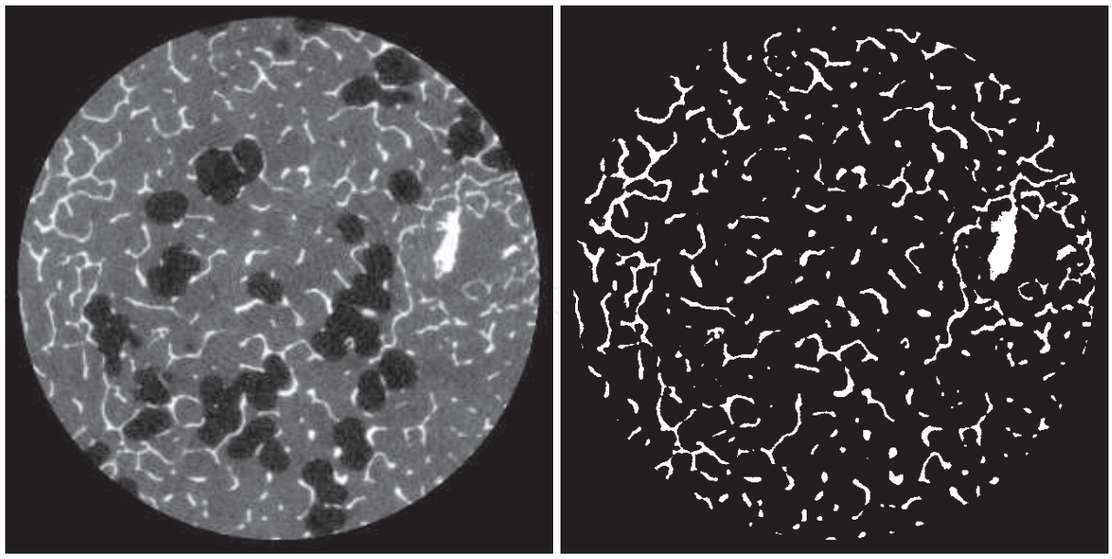

(a) (b)

Fig. 10. (a)Extracted Core image (b)Binary image after thresholding

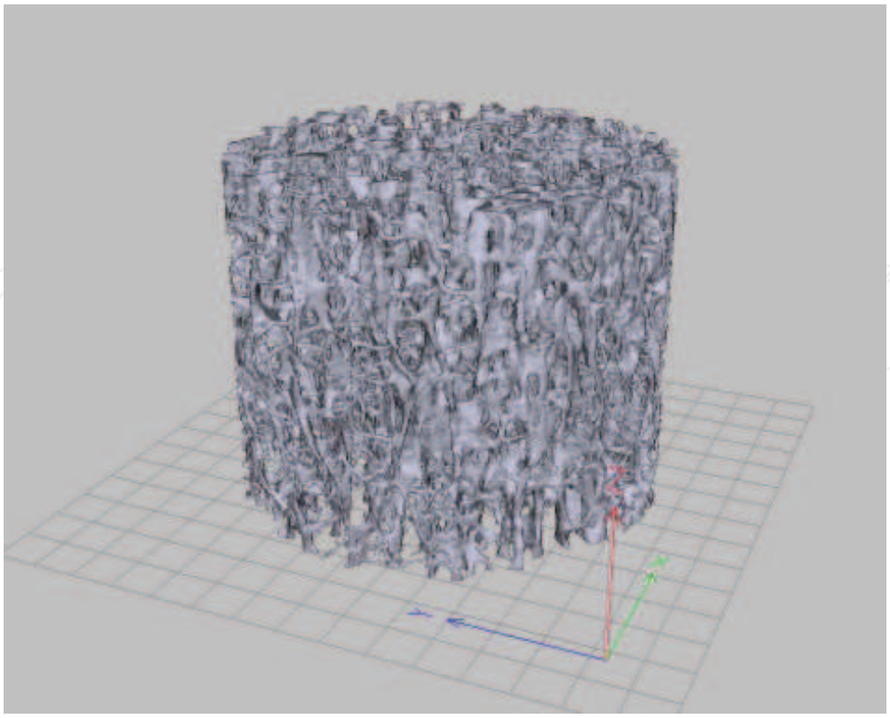

Fig. 11. Surface model of the segmented core

5. Quantification

The calculated midaxis is shown overlapped on to the original section of cancellous bone in Figure 12(a). The blue voxels represent the rods and the red voxels represent the plates. The midaxis of the rods are segmented in to individual struts and their orientation is calculated. These are then classified as horizontal strut (if the orientation is less than 45 degrees with respect to the horizontal plane) or vertical struts (if the orientation is $\geq$45 degrees). This is shown in Figure 12(b).

Several small sections of bone were extracted from the 4th Lumbar vertebra core. The parameters to quantify the bone were calculated on these sections. These sections were

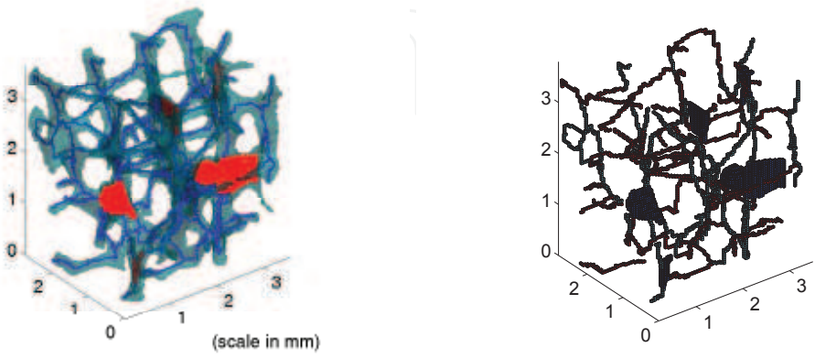

(a) (b)

Fig. 12. (a) Cancellous bone overlapped on the medial axis. (b) Orientation of the rods. Cyan voxels represent the vertical struts.

	Dataset1	Dataset2	Dataset3	Dataset4	Clinical Study (Mean)	SD
rTb.Th (mm)	0.1202	0.1121	0.1186	0.0919	0.139	0.028
pTb.Th (mm)	0.1498	0.1262	0.1381	0.1034	0.139	0.028
Tb.Sp (mm)	0.13	0.1126	0.0694	0.0973	0.854	0.143
Tb.N (mm^{-1})	2.788	3.3931	4.9932	2.8502	1.161	0.181
BV/TV (%)	12.1537	33.5976	17.2474	12.3187	8.7	0.033
BS/BV (mm^{-1})	22.0369	9.7129	30.2927	28.1630	21.17	3.59

Table 1. Calculated parameters compared to Hildebrand et al. (Hildebrand et al., 1999)

approximately $3mm^3$ in size. Calculations were done on these smaller sections because of the computational power needed to do it on the whole core. Tools like the Mathwork's Distributed Computing Server/Parallel Computing toolbox (*http://www.mathworks.com/*, Nov 2010) can be used to do the calculations on the whole core. These parameters are listed in Table 1. The column, Clinical Study, shows the data collected form 52 donars in a clinical study (Hildebrand et al., 1999). It shows the mean and the standard deviation (SD) of the values calculated on the whole 4th Lumbar vertebra. The Figure 13 shows the comparison between the clinical data and the calculated parameters on the sections extracted form the core.
The remodeling algorithm was applied on a section extracted from the core. The load signal generated by LifeMOD (LifeModeler Inc. San Clemente, California) was used for this experiment. This illustrates the ability to use the real world motion data to drive the remodeling algorithm. The results of this simulation are shown in Figure 14. The top row is the principal stress, middle row is the strain energy density and the bottom row is the geometry of the trabecular bone. Column (a) is the initial geometry, column (b) is the configuration after 7 iterations and column (c) is configuration after 14 iterations.

6. Virtual reality visualization

An initial effort has been made to facilitate interactive navigation through the complex 3D geometry of the cancellous bone structure using human computer interfaces, e.g., gyro mouse and stereoscopic head mounted display with Intersense-based head tracking. The resulting visualization facilitates more efficient study of the complex biological structures. For example, the original and the aged bone can be interactively viewed/navigated, the results of the FEA can be texture-mapped onto the 3D geometry of the bone to augment the researcher's ability to identify the stress localization in bone structure. Virtools, a virtual reality simulation and modeling software, was used for interactive visualization and navigation. A screen shot of the cancellous bone in the virtual environment is shown Figure 15.

7. Conclusion

The proposed method can be used to produce a subject-specific structure. The generated structure can be used to predict the effect on the overall trabecular bone structure (e.g., strength of the bone). Based on these results the loading conditions on the bone can be changed to produce more desirable results, i.e., stronger or at least not a weak structure. This can have applications in physiotherapy, help avoid injuries in various sports and study the effects of different types of bone implants over a period of time.

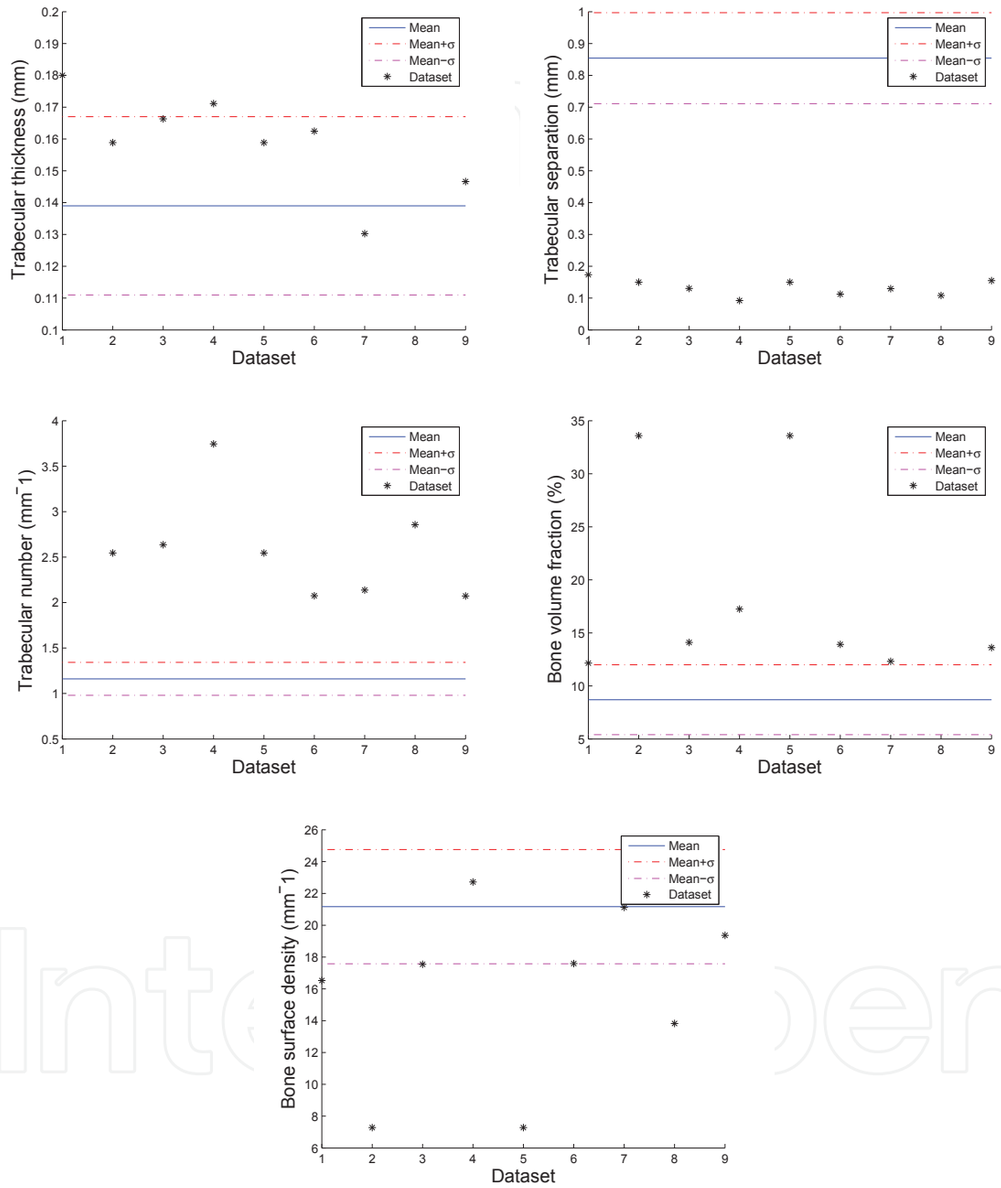

Fig. 13. Comparison of the calculated parameters (∗) in comparison with the clinical data (blue, red, magenta lines)

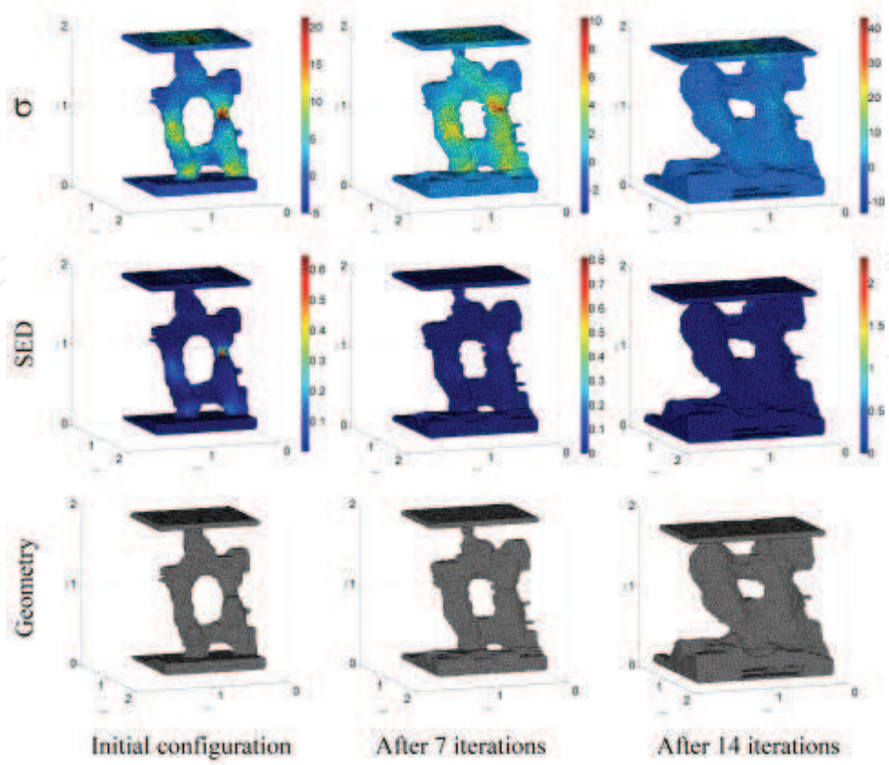

Fig. 14. Results of remodeling algorithm simulation (a) initial geometry (b) after 7 iterations (c) after 14 iterations

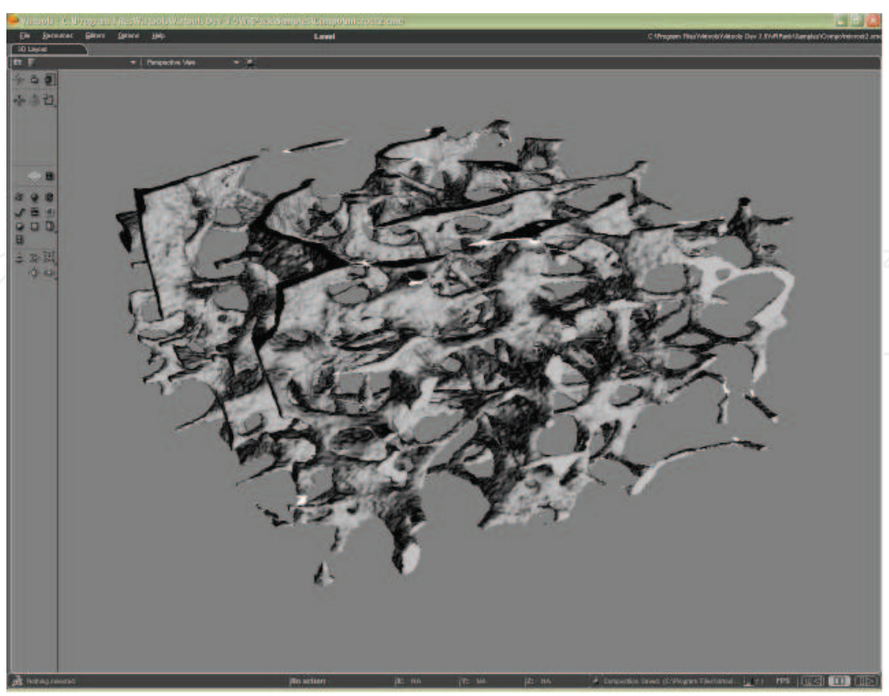

Fig. 15. Virtual reality visualization of the cancellous bone

8. References

Bronckers, A., Goei, W., Luo, G., Karsenty, G., D'Souza, R., Lyaruu, D. & Burger, E. (1996). DNA fragmentation during bone formation in neonatal rodents assessed by transferase-mediated end labeling., *Journal of bone and mineral research: the official journal of the American Society for Bone and Mineral Research* 11(9): 1281.

Burger, E. & Klein-Nulend, J. (1999). Mechanotransduction in bone-role of the lacuno-canalicular network, *The FASEB Journal* 13(9001): 101.

Burr, D. (1993). Remodeling and the repair of fatigue damage, *Calcified tissue international* 53: 75–81.

Burr, D. (2002). Targeted and nontargeted remodeling, *Bone* 30(1): 2–4.

Frost, H. (1982). Mechanical determinants of bone modeling., *Metabolic bone disease & related research* 4(4): 217.

Frost, H. (1983). A determinant of bone architecture: the minimum effective strain, *Clinical Orthopaedics and Related Research* 175: 286.

Hildebrand, T., Laib, A., Müller, R., Dequeker, J. & Rüegsegger, P. (1999). Direct three-dimensional morphometric analysis of human cancellous bone: microstructural data from spine, femur, iliac crest, and calcaneus, *Journal of Bone and Mineral Research* 14: 1167–1174.

Hildebrand, T. & Ruegsegger, P. (1997). A new method for the model-independent assessment of thickness in three-dimensional images, *Journal of Microscopy* 185(1): 67–75.

http://iso2mesh.sourceforge.net/cgi-bin/index.cgi (n.d.).

http://www.mathworks.com/ (Nov 2010).

Huiskes, R., Ruimerman, R., van Lenthe, G. & Janssen, J. (2000). Effects of mechanical forces on maintenance and adaptation of form in trabecular bone, *Nature* 405(6787): 704–706.

Ju, T., Baker, M. & Chiu, W. (2007). Computing a family of skeletons of volumetric models for shape description, *Computer-Aided Design* 39(5): 352–360.

Lemaire, V., Tobin, F., Greller, L., Cho, C. & Suva, L. (2004). Modeling the interactions between osteoblast and osteoclast activities in bone remodeling, *Journal of theoretical biology* 229(3): 293–309.

Linden, J., Verhaar, J., Pols, H. & Weinans, H. (2003). A simulation model at trabecular level to predict effects of antiresorptive treatment after menopause, *Calcified tissue international* 73(6): 537–544.

Liu, X., Huang, A., Zhang, X., Sajda, P., Ji, B. & Guo, X. (2008). Dynamic simulation of three dimensional architectural and mechanical alterations in human trabecular bone during menopause, *Bone* 43(2): 292–301.

Mosekilde, L. (1988). Age-related changes in vertebral trabecular bone architecture–assessed by a new method., *Bone* 9(4): 247–50.

Mosekilde, L. (1989). Sex differences in age-related loss of vertebral trabecular bone mass and structure–biomechanical consequences., *Bone* 10(6): 425.

Mullender, M. & Huiskes, R. (1995). Proposal for the regulatory mechanism of Wolff's law, *Journal of orthopaedic research* 13(4): 503–512.

Müller, R. & Hayes, W. (1997). Biomechanical competence of microstructural bone in the progress of adaptive bone remodeling, *Proceedings of SPIE*, Vol. 3149, SPIE, p. 69.

Müller, R. & Rüegsegger, P. (1996). Analysis of mechanical properties of cancellous bone under conditions of simulated bone atrophy, *Journal of Biomechanics* 29(8): 1053–1060.

Parfitt, A. (1984). The cellular basis of bone remodeling: The quantum concept reexamined in light of recent advances in the cell biology of bone, *Calcified Tissue International*

36: 37–45.
Parfitt, A., Drezner, M., Glorieux, F., Kanis, J., Malluche, H., Meunier, P., Ott, S. & Recker, R. (1987). Bone histomorphometry: Standardization of nomenclature, symbols, and units, *J Bone Miner Res* 2(6): 595–610.
Parfitt, A., Mathews, C., Villanueva, A., Kleerekoper, M., Frame, B. & Rao, D. (1983). Relationships between surface, volume, and thickness of iliac trabecular bone in aging and in osteoporosis. Implications for the microanatomic and cellular mechanisms of bone loss., *Journal of Clinical Investigation* 72(4): 1396.
Pivonka, P., Zimak, J., Smith, D., Gardiner, B., Dunstan, C., Sims, N., John Martin, T. & Mundy, G. (2008). Model structure and control of bone remodeling: A theoretical study, *Bone* 43(2): 249–263.
Rüegsegger, P., Koller, B. & Müller, R. (1996). A microtomographic system for the nondestructive evaluation of bone architecture, *Calcified tissue international* 58(1): 24–29.
Ruimerman, R., Huiskes, R., Van Lenthe, G. & Janssen, J. (2001). A computer-simulation model relating bone-cell metabolism to mechanical adaptation of trabecular architecture, *Computer Methods in Biomechanics and Biomedical Engineering* 4(5): 433–448.
Simmons, C. & Hipp, J. (1997). Method-Based Differences in the Automated Analysis of the Three-Dimensional Morphology of Trabecular Bone, *Journal of Bone and Mineral Research* 12(6): 942–947.
Sommerville, D. (1959). *Analytical geometry of three dimensions*, The University Press.
Stauber, M. & Müller, R. (2006). Volumetric spatial decomposition of trabecular bone into rods and plates - A new method for local bone morphometry, *Bone* 38(4): 475–484.
Thomsen, J., Laib, A., Koller, B., Prohaska, S., Mosekilde, L. & Gowin, W. (2005). Stereological measures of trabecular bone structure: comparison of 3D micro computed tomography with 2D histological sections in human proximal tibial bone biopsies, *Journal of Microscopy* 218(2): 171–179.
Van Der Linden, J., Verhaar, J. & Weinans, H. (2001). A Three-Dimensional Simulation of Age-Related Remodeling in Trabecular Bone, *J Bone Miner Res* 16(4): 688–696.
Van Rietbergen, B., Huiskes, R., Weinans, H., Sumner, D., Turner, T. & Galante, J. (1993). The mechanism of bone remodeling and resorption around press-fitted THA stems, *Journal of biomechanics* 26(4-5): 369–382.
Weinbaum, S., Cowin, S. & Zeng, Y. (1994). A model for the excitation of osteocytes by mechanical loading-induced bone fluid shear stresses, *Journal of biomechanics* 27(3): 339–360.
Wolff, J. (1986). The Law of Bone Remodeling.(Das Gesetz der Transformation der Knochen, Kirschwald, 1892). Translated by Maquet, P., Furlong, R.

Virtual Reality

Edited by Prof. Jae-Jin Kim

ISBN 978-953-307-518-1
Hard cover, 684 pages
Publisher InTech
Published online 08, December, 2010
Published in print edition December, 2010

Technological advancement in graphics and other human motion tracking hardware has promoted pushing "virtual reality" closer to "reality" and thus usage of virtual reality has been extended to various fields. The most typical fields for the application of virtual reality are medicine and engineering. The reviews in this book describe the latest virtual reality-related knowledge in these two fields such as: advanced human-computer interaction and virtual reality technologies, evaluation tools for cognition and behavior, medical and surgical treatment, neuroscience and neuro-rehabilitation, assistant tools for overcoming mental illnesses, educational and industrial uses In addition, the considerations for virtual worlds in human society are discussed. This book will serve as a state-of-the-art resource for researchers who are interested in developing a beneficial technology for human society.

How to reference

In order to correctly reference this scholarly work, feel free to copy and paste the following:

Ajay Sonar, Laurel Kuxhaus and James Carroll (2010). Simulation of Subject Specific Bone Remodeling and Virtual Reality Visualization, Virtual Reality, Prof. Jae-Jin Kim (Ed.), ISBN: 978-953-307-518-1, InTech, Available from: http://www.intechopen.com/books/virtual-reality/simulation-of-subject-specific-bone-remodeling-and-virtual-reality-visualization

INTECH
open science | open minds

InTech Europe
University Campus STeP Ri
Slavka Krautzeka 83/A
51000 Rijeka, Croatia
Phone: +385 (51) 770 447
Fax: +385 (51) 686 166
www.intechopen.com

InTech China
Unit 405, Office Block, Hotel Equatorial Shanghai
No.65, Yan An Road (West), Shanghai, 200040, China
中国上海市延安西路65号上海国际贵都大饭店办公楼405单元
Phone: +86-21-62489820
Fax: +86-21-62489821

© 2011 The Author(s). Licensee IntechOpen. This chapter is distributed under the terms of the Creative Commons Attribution-NonCommercial-ShareAlike-3.0 License, which permits use, distribution and reproduction for non-commercial purposes, provided the original is properly cited and derivative works building on this content are distributed under the same license.

IntechOpen

IntechOpen